MEDWIN PUBLISHERS
Committed to Create Value for Researchers

Nanomedicine & Nanotechnology Open Access
ISSN: 2574-187X

Curvature Optimised Plasmonic Gold-Gallium Oxide Nanocomposites for High Temperature Optical Detection of NO_2

Keerthana L, Dharanya C and Dharmalingam G*

Plasmonic nanomaterials laboratory, PSG Institute of Advanced Studies, Coimbatore-641004, India

***Corresponding author:** Gnanaprakash Dharmalingam, Plasmonic nanomaterials laboratory, PSG Institute of Advanced Studies, Coimbatore-641004, India, Email: dgp@psgias.ac.in

Research Article

Volume 8 Issue 2

Received Date: May 19, 2023

Published Date: June 30, 2023

DOI: 10.23880/nnoa-16000235

Abstract

NO_2 emissions are of great concern to human health, with projected increases in consumption of its sources making it vital to develop sensors for monitoring its production in harsh environment such as combustion sources. Plasmonic nanomaterials can be extremely sensitive and hence useful in this regard, but suffer from inherent thermal stability drawbacks. The plasmonic and morphological characteristics of mixed polygon incorporated gallium oxide nanocomposites and their dependence on the changes in surrounding environment on gas exposure has been investigated here. We have detected NO_2 at high temperature (800°C) by monitoring the change in intensity of the surface plasmon at the interfaces of the gold gallia nanocomposite as a function of time for different concentrations. The results obtained in this study demonstrates that it is a promising sensing material to detect oxidizing gases like NO_2.

Keywords: Plasmonics; Gold Nanopolygons; High Temperature Sensing; NO_2; Temperature Stability

Introduction

Nanotechnology has undoubtedly led to considerable enhancements to existing material properties as well as to discoveries of emerging phenomena in a multitude of materials and material classes. The optical properties and specifically the extinction of light by nanomaterials has been considerably imbibed with additional flexibilities as a consequence. A very interesting and quite comprehensively studied subdivision of optical property manipulation is the field of plasmonics. The behaviour of collective excitations of free electrons (plasmons) in response to multiple influencers including but not limited to material composition, morphology and environment can be very pertinent and suitable for multiple applications such as displays [1] sensors [2] catalysis [3] energy storage, field emission [4] lasing, communication and the like [5]. Plasmonics as an arena of research hinges on the electromagnetic field concentrations due to the highly localized confinement of the plasmons, and specifically the sensitivity of this concentrated field to the proximal environment. One area of direct relevance to plasmon derived material property enhancements is high temperature catalysis and more specifically, sensing of gases at high temperature. The requirement of absolute chemical and dimensional (morphological) stability is a tough to fulfil pre-requisite of high temperature gas sensing. Plasmonic materials have sensitivities directly proportional to their curvature, as higher curvatures lead to higher field enhancements due to more effective plasmon localizations [6-9]. However, structures with high curvature suffer from a

more primitive limitation of having a reduced shape stability with increasing temperature due to the inherent propensity towards surface energy minimization and the resulting progression towards rounder shapes. Studies done by us and other groups have revealed this phenomenon, wherein nanorods having higher sensitivities than spheres become spheres with increasing temperature, with an increasing tendency towards spheroidization with an increasing curvature [5,10-14]. There can hence be a structure envisioned to exist that provides an optimal compromise between high field localizations and shape stability for a particular temperature (other factors such as the sensing environment and material composition held constant). In this work, we have synthesized through a microwave based process mixed polygons of Au (AuPs) comprising of triangles and hexagons with differing degrees of polygonality. To stabilize them effectively against a change in morphology, we have composited them with Gallium Oxide (AG), a well-known support for plasmonic materials from our previous studies. We have investigated the feasibility of these materials as sensing materials for NO2, a common gas encountered in combustion environments, at temperatures of 800°C. Though NO2 itself is an optical absorber, we have de-convoluted the response towards it by our sample by a statistical analysis procedure. The results presented herein along with the validation of morphological and chemical stabilities of the investigated nanocomposites make them as a pertinent choice in the field of plasmonic high temperature gas sensing.

Materials And Methods

Chloroauric acid ($HAuCl_4$), sodium thiosulfate ($Na_2S_2O_3$), gallium nitrate ($GaNO_3$), were purchased from Sigma Aldrich (99.0% pure) and used without further purification. The experiments were carried out using distilled water.

Preparation of AuPs

AuPs were prepared by mixing 5mL of 2mM chloroauric acid solution with10mL of distilled water along with 5mL of 1mM sodium thiosulfate. This solution was irradiated under microwave for 4 min at 425W. The resulting solution appeared deep brown. The solution obtained was further centrifuged at 10,000rpm for 10 min with isopropanol and water for removal of unreacted species in the reaction mixture until the achievement of a neutral pH.

Preparation of AG

To synthesize AG nanocomposites, 10mL of the synthesized AuPs were added to 10mL of a 1mM gallium nitrate aqueous solution and introduced into a microwave reactor. The sample was irradiated for four minutes with 425W of power and subsequently transferred to a hydrothermal reactor and heated at 180ºC for 8h. Finally, the product was washed several times with water and centrifuged at 10000rpm. The nanoparticles were then suspended in IPA and spun on a quartz substrate at 1500rpm, dried at 90ºC and then annealed at 900ºC. The formation mechanism of the nanocomposite through the hybrid microwave and hydrothermal process is given below.

$$HAuCl_4 + Na_2S_2O_3.2H_2O \rightarrow Au^0 + 2H_2O + 2NaCl + 2HCL \quad (1)$$

$$Au^0 + GaNO_3 \xrightarrow[8h]{180^0} GaOOH \xrightarrow[1h]{800^0} AG \quad (2)$$

Thermal stability studies on AuPs and AG

Thermal stability tests were performed by monitoring wavelength and intensity (*in-situ*) through UV-VIS spectroscopy of the synthesized AuPs as well as the nanocomposites. For these tests the procedure followed was: (i) the resultant solution of AuPs (obtained from the microwave process) as well as AG (obtained from the hydrothermal approach) being spun on a quartz substrate (15layers) (ii) the substrates being annealed at 800ºC (iii) post annealing, monitoring the substrates to confirm the presence of and changes in Au in AuPs as well as AG nanocomposites using UV-Visible spectroscopy. Thermal stability tests were performed by monitoring the optical absorbance over the wavelength range of 350nm-1000nm using a Flame spectrometer from Ocean Optics. AuPs and AG spun on quartz substrates were placed inside a high temperature furnace, and heated to 800°C at a ramp rate of 10°C/min with constant exposure to air (2SLPM flowrate) over a period of 2h. Light from a tungsten halogen source of wavelength 300-2000nm (HL-2000 from Ocean optics) was passed through the film, and the transmitted light was collected using a collimating lens coupled with an optical fibre cable that fed into the flame spectrophotometer.

Characterization

The nanostructures synthesized were characterized using a Flame-T-Visible spectrometer (Ocean optics) coupled with a halogen light source (HL-2000 from ocean optics) with associated beam optics. Transmission electron microscopy (TEM) images and Energy dispersive X-ray spectra (EDS) were collected using a JOEL JEM 2100 with 200kV accelerating voltage to study the morphological aspects of the synthesized nanocomposites. For TEM, the colloidal suspensions were coated on copper grids and dried at room temperature. The crystalline structure of AG nanocomposites were investigated by X-ray diffraction (XRD) using an Empyrean, Malvern Panalytical instrument with Cu-Kα source radiation, (λ=1.54Aº). The diffractograms

were recorded between 2θ angles of 20º and 90º.

Results And Discussion

The section discussing the observations from our investigations on the fabricated nanocomposites has been divided as follows. Initially, the results from characterization of the synthesized materials has been presented. We then postulate a mechanism for the formation of the highly assorted polygons based on our observations. Followed by this, the results from our assessments of the stability in morphology of only AuPs and the nanocomposites has been elucidated. Finally, we present our findings on the sensing properties of the fabricated nanocomposites when subject to the analyte of NO_2 at a temperature of 800°C.

Morphological structural and compositional properties of AuPs and AG

Optical properties

Surface plasmon resonance is as explained briefly in preceding sections a highly sensitive property with respect to particle morphological changes. The monitoring of the optical absorbance hence can give vital clues which other techniques can seldom provide. With this reasoning, the absorbance properties of the nanocomposites were studied. The optical absorption spectra of AuPs and AG are presented in figure 1 and figure 2 respectively. AuPs were prepared by the reduction of Au (III) ions to Au (0) in the presence of sodium thiosulphate as a reducing agent. Figure 1a depicts the absorption peaks of AuPs exhibiting two plasmonic peaks at 530nm and 790nm. AuPs were then spun on quartz substrate for which the peak has shifted towards a shorter wavelength (1b). This is presumed to be due to particle aggregation due to interactions with the substrate and due to the drying process, leading to a considerable damping of the red-shifted peak. When this substrate was annealed at 800ºC the sample shows a disappearing of the longitudinal plasmonic peak (1c) which can be attributed to thermal expansion and associated free electron density decrease which will also cause and additional red shift along with the damping. Post annealing at room temperature the AuPs exhibited a red shift of 15nm (compared to 1b) with an associated decrease in intensity of the absorption peak which is in agreement with the literature [15]. Briefly, the reasons for the red shift are postulated to be due to a change in the morphology of the polygons which could not be imaged in TEM as the structures were dispersed in a quartz substrate and were not able to be recovered and re-dispersed on TEM imaging grids.

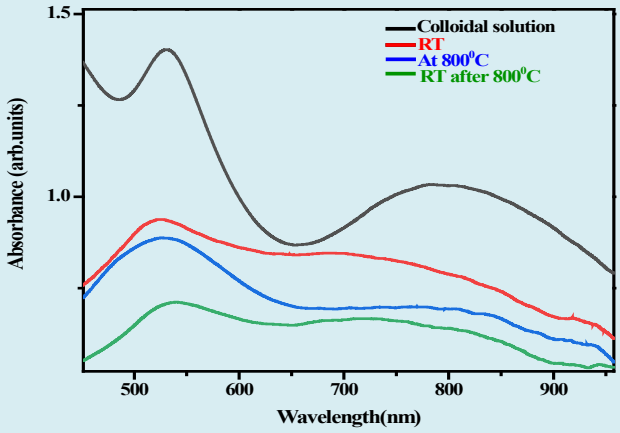

Figure 1: optical absorbance of (a) AuPs as a colloidal solution (black) (b) AuPs coated on a substrate at room temperature (red) (c) AuPs at 800ºC (blue) and (d) AuPs post thermal stability at room temperature (green).

Pristine AuPs are hence envisaged to undergo agglomeration and/or changes in morphology during thermal annealing which can be unfavourable to the sensing performance as it changes and degrades the plasmonic properties. AuPs incorporated in a metal oxide matrix (GaO), are expected to be better stabilized against agglomeration/ morphological change as revealed by our recent findings [16,17]. As can be observed from the resulting optical characterization studies on AG, similar experiments on a substrate reveal that the degree of changes to the optical absorption has been minimized when AuPs are composited with GaO with a red shift of only 8nm (at 800°C) and that too only during the first high temperature treatment. Post annealing at room temperature the peak has a shift of about 4nm.

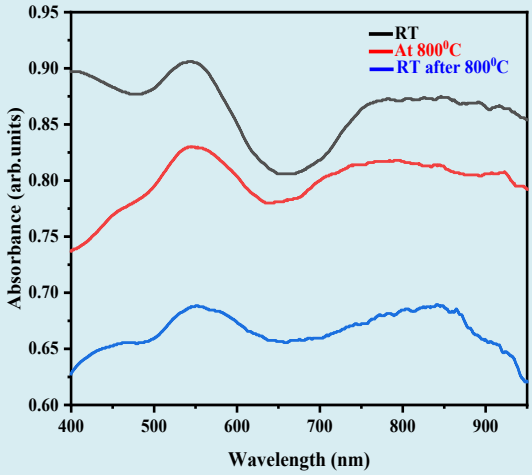

Figure 2: Optical absorbance of AG (a) at room temperature (black) (b) at 800ºC (red) (c) post thermal stability at room temperature (blue).

Structural studies on the synthesized nanomaterials

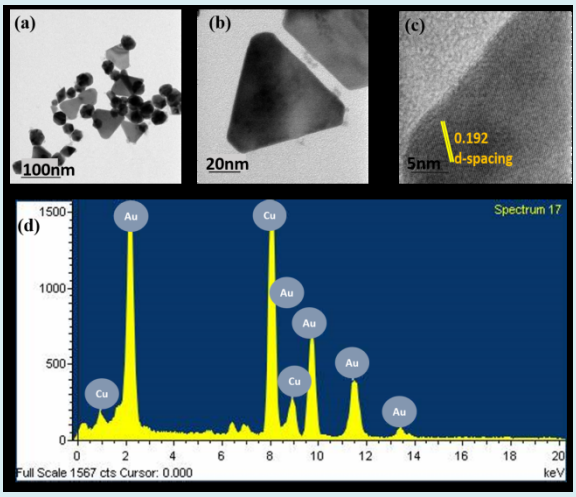

Figure 3: TEM image of AuPs which exhibits a mixed morphology of triangles and other polygons ((a) and (b)). (c) d-spacing illustration and (d) EDS spectrum of AuPs .

It is clear from the TEM images that the particles formed are mixed shapes of smaller icosahedral and larger truncated prisms and higher polygons. Since the particle size (taken from 25 measurements) of truncated prisms are larger (56±45nm) than icosahedrons (37±25nm), two plasmonic peaks are observed as shown in figure 1(a) as evidenced prior and confirmed by other studies [17]. The d-spacing has been calculated to be 0.192 using ImageJ software. The EDS analysis shows the presence of AuPs with no other impurities traced. We propose a mechanism below for the formation of such mixed morphologies, which are of considerable interest in multiple plasmonic investigations and applications.

Compositional analysis on the synthesized nanocomposites

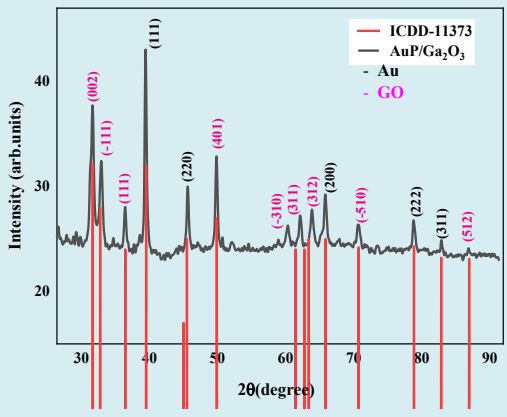

Figure 4: Diffraction pattern of AG.

The composition of the fabricated composites was analysed and corroborated through XRD. The phase formation of β-GaO was a primary confirmation from XRD, as shown in figure 4. Here, the lattice planes (111), (200), (220), (311) and (222) correspond to the characteristic peaks of face centered cubic Au. β- GaO with the lattice planes of (111), (200), (220), (311) and (002), (-111), (111), (401), (-310),

(311), (312), (-510) and (512) has been observed. We have in our previous studies reported the ability to tune the phase of GaO between α, β, and δ through a controlled evolution of morphology [18]. From other studies on hydrothermally synthesized GaO reported previously, the innate tendency for the formation of the β phase when there is morphology directing mechanism present has been reaffirmed here [16]. Based on the findings so far, we postulate a mechanism for the formation of the observed morphologies and compositions of the mixed polygons of Au and GaO.

Formation mechanism of AG

Sodium Thiosulfate ($Na_2S_2O_3$) is one of the interesting anionic surfactants that facilitates anisotropic growth of nanoparticles. Kim et al has synthesized Te nanowires using $Na_2S_2O_3$ and investigated the effect of $Na_2S_2O_3$ on the morphology and size. Concentrations were when increased from 0.2g-1g, wherein at the higher concentrations mixed morphologies of hexagons and tubes whereas at lower concentrations only tubes were observed [19]. In our study, we observe polygons mostly consisting of larger prisms and an equal proportion of higher order polygons of hexagons, pentagons and octagons since $Na_2S_2O_3$ could be selectively adsorbed on the facets of Au particles, thereby serving as a growth directing agent. The proposed growth mechanism is illustrated as shown in Figure 5.

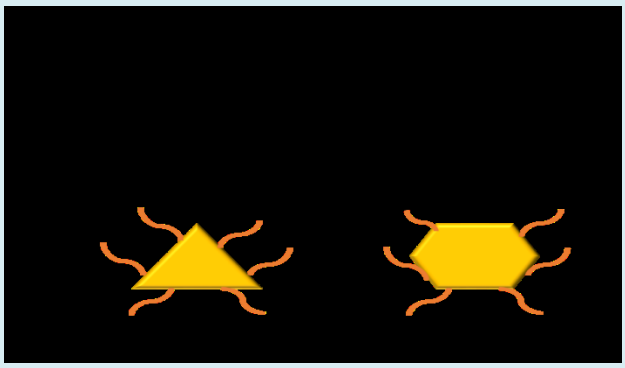

Figure 5: Mechanism of formation of mixed polygonal structures of Au comprising of truncated prisms and hexagons.

High temperature Gas sensing measurements and data acquisition

Optical gas sensing tests were performed by monitoring the plasmonic absorbance over the wavelength range of 350nm-1000nm at 800°C. AG spun on quartz substrates was placed inside a high temperature furnace, and different concentrations of NO_2 was exposed using Alicat Scientific mass flow controllers (MFC). In a typical NO_2 sensing experiment, the sample was first heated to 800°C at a ramp rate of 10°C/min with constant exposure to air (2SLPM flowrate) over a period of 2h and was held at this condition for 30min prior to the first gas exposure. Post this ramping and stabilization step, AG was exposed to three different concentrations of NO_2 viz., 1000ppm, 2000ppm and 5000ppm. Each of the concentrations were exposed thrice and the individual gas exposures were for 5min. Light from a tungsten halogen source of wavelength 300-2000nm (HL-2000 from Ocean optics) was passed through the film, and the transmitted light was collected using a collimating lens coupled with an optical fibre cable that fed into a spectrophotometer. Once the data acquisition was completed, the change in intensity as a function of time for different wavelengths (500-950nm) was plotted using python program.

Gas kinetics of NO_2 at high temperature

NO_2 is a polar molecule due to the presence of lone pair of electrons on nitrogen whose electron- electron repulsion results in a trigonal planar structure. It is made of sigma/covalent bonds formed by the head-head overlap of atomic orbitals. This inequality develops a charge within the molecule promoting the persistence of a permanent dipole. When light passes through molecule, transitions from bonding to non-bonding/anti-bonding orbital in the visible region since nitrogen has a lone pair of electrons. With regards to the reaction mechanism of NO_2 the one unpaired electron in nitrogen makes it very reactive, dimerising it to attain stability and forming N_2O_4. N_2O_4 does not have unpaired electrons but consists of two sigma and two pi-bonds, comprising ultimately of four resonance capable entities. First resonance occurs in the near UV around 340nm (3.6eV). Due to instrumental limitations, absorbance in this region cannot be investigated and hence is not included in this study. The other absorptions occur in the visible region. Upon increasing the temperature to 800°C, the equilibrium tends to shift towards producing more NO_2 gas molecules (endothermic reaction) and upon cooling the equilibrium shifts backward again producing more N_2O_4 molecules (exothermic reaction). When the gas molecules are heated, the volume of the gas also increases and kinetics is increased according to the ideal gas law, PV=nRT. Also the number of molecules/population of molecules decreases with increase in temperature in the testing chamber. Due to the inherent NO_2 absorption in the visible region, AG like composites whose plasmon band peaking beyond 650nm can be used as a coherent choice.

Response of AG towards NO_2

At 800ºC the reactive oxygen species (O^- and O^{2-}) during the temperature ramping stages of the experiment are chemisorbed on the surface of AG or AuPs, followed by migration into the oxygen vacancy sites. This results in either a decrease in polarizability of the GaO or a decrease

in the free electron density of AuPs, and a net change in plasmon frequency depending on which of these phenomena dominate. The reaction pathway can be written as:

$$O_{2(g)} + Vo_{(s)} + Ga^{3+}{}_{(s)} \rightarrow O_{2\ (ads)} + Ga^{4+}{}_{(s)} \quad (3)$$

(or)

$$O_{2(g)} + Vo_{(s)} + Au_{(s)} \rightarrow O_{2(ads)} + Au^{2+}{}_{(s)} \quad (4)$$

$$O_{2(ads)} + V_{O(b)} \rightarrow O_{2(b)} \quad (5)$$

Where subscripts g, s, b and ads denote gas phase, surface, bulk and adsorbed states respectively. Oxygen vacancies are filled through charge transfer between adsorbing oxygen, vacancy sites and AuPs, during exposure to air atmosphere.

NO_2 has been detected here by exploiting the significantly improved (compared to lower temperatures) oxygen ion conduction properties of GaO that has been reported to commence at 650ºC and the catalytic reactivity promoted by the plasmonic property of Au. From the UV analysis it can be seen that AG has a distinct plasmonic signature beyond 650nm whose peak position is extremely sensitive to changes in surrounding environment, making the nanocomposite ideal to detect NO_2. Upon NO_2 exposure, the gas molecules dissociate into NO^- and O^- ions and the O^- ions find unoccupied vacancy/defect sites on the surface for adsorption/adsorption + migration [20]. The reaction pathway can be written as follows:

$$NO_2 \rightarrow NO^-{}_{(ads)} + O^-{}_{(ads)} \quad (6)$$

As shown in figure 6 (a) the intensity of the peaks at all three concentrations has decreased, with increase in wavelength and intensity of the peaks becoming the highest for 5000ppm. It is also evident that changes to the intensity peaks are observed beyond 650nm-800nm for 2000ppm and 5000ppm. This could be attributed to the conversion of NO_2 to NO reactions occurring within nanocomposite as explained in equation (4) and (5). Figure 6 (b) indicates the difference in intensity when NO_2 alone was purged (denoted as raw absorbance) whereas when the sample was present during the NO_2 exposure (AG) for the representative concentration of 1000ppm at a representative wavelength of 400nm. It is hence conclusive that the difference in the intensities could be due to reactions between sample and gas, in which the NO_2 gas molecules has been converted to NO. The precise events that lead to the observed quenching of intensities in relation to and in addition to the proposed mechanisms are subject for scrutiny for follow-on studies. Calibration curves showing the differences in the intensity changes when only NO_2 was purged whereas when the sample was present during the NO_2 purge were determined for 1000ppm and 5000ppm and are shown in figure 6(c). It is clear the most responsive wavelength (considering the plasmonic region of 500nm-900nm) is 500nm for 5000ppm and 1000ppm which comes under the plasmonic regime of the sample, implying a plasmonic contribution to the observed changes on NO_2 exposure.

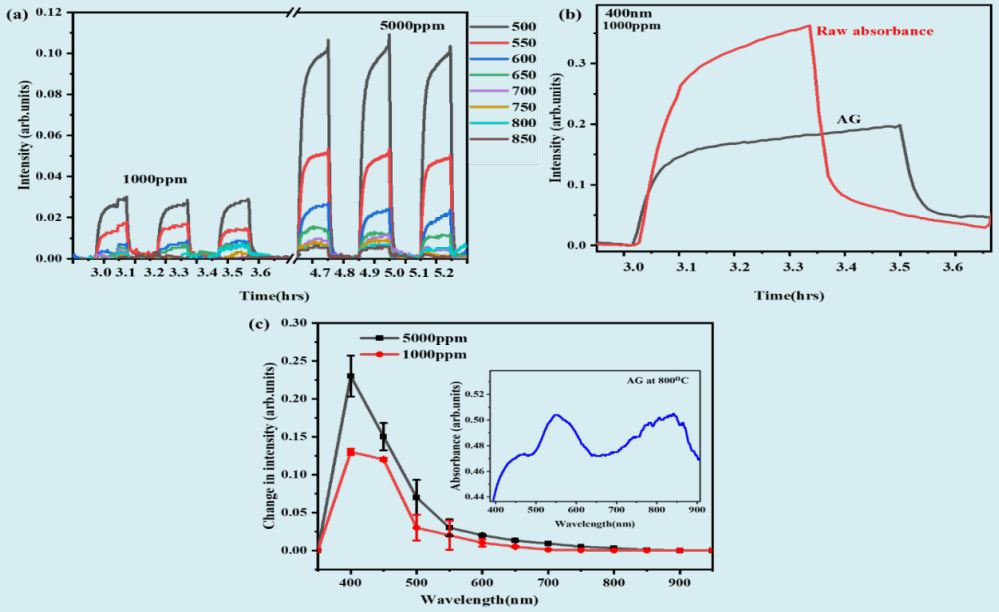

Figure 6(a): Response to NO_2 as a function of intensity at different wavelengths from the range of 450nm-850nm of the AG sample (b) Graph depicting the absorption intensity changes in response towards only NO_2 whereas when AG was present during the exposure (c) Difference in absorbance intensity of AG vs only NO_2 from the entire investigated UV-visible spectrum.

Conclusions

In this work, we have investigated nanocomposites of mixed Au polygons- and gallia synthesized through a solution process to detect NO_2 at 800°C for the first time. We have postulated a growth mechanism that will allow the formation of such mixed polygons through microwave irradiation and a thiosulfate growth director. From UV-visible studies of AG only a minor shift has been observed as it is evident that the GaO has mitigated agglomeration/ change in morphology of the polygons thereby preserving the plasmonic property enhancements. The thermal stability of the nanocomposites for 2h is a prominent result in that they can be used as a sensing material to detect NO_2 emissions. Future work aimed at temperature dependent studies, improving the stability of the nanocomposite for prolonged exposure to such high temperatures as well as optimizing the shape and size distribution of the polygons are under way to comprehensively study such material combinations for plasmonic applications such as sensing and catalysis.

Conflicts Of Interest/ Competing Interest

The authors declarer that there is no conflict of interest.

Acknowledgements:

The authors gratefully acknowledge support received from the Materials & Manufacturing panel of the Aeronautics Research & Development Board, Govt of India, Sanction code: DGTM/TM/ARDB/GIA/18-19/0296, (Project No: 2031895).

References

1. Sharifi M, Attar F, Saboury AA, Akhtari K, Hooshmand N, et al. (2019) Plasmonic gold nanoparticles: Optical manipulation, imaging, drug delivery and therapy. J Control Release 311-312: 170-189.

2. Peeters H, Keulemans M, Lenaerts S, Verbruggen SW (2020) Photocatalytic self-cleaning coatings with embedded gold nanoparticles 1-28.

3. Wang B, Zhu X, Li S, Chen M, Liu N, et al. (2019) Enhancing the photovoltaic performance of perovskite solar cells using plasmonic Au@Pt@Au core-shell nanoparticles. Nanomaterials 9(9).

4. Huang X, Jain PK, El Sayed IH, El Sayed MA (2008) Plasmonic photothermal therapy (PPTT) using gold nanoparticles. Lasers Med Sci 23: 217-228.

5. Chen M, He Y, Wang X, Hu Y (2018) Numerically investigating the optical properties of plasmonic metallic nanoparticles for effective solar absorption and heating. Sol Energy 161: 17-24.

6. Keerthana L, Ahmad Dar M, Dharmalingam G (2021) Plasmonic Au-Metal Oxide Nanocomposites for High-Temperature and Harsh Environment Sensing Applications. Chem An Asian J 16(22): 3558-3584.

7. Narayanan K, Gnanaprakash D (2022) Branched Gold Nanostructures Through a Facile Fructose Mediated Microwave Route. J Clust Sci 33: 227-240.

8. Xi W, Phan HT, Haes AJ (2018) How to accurately predict solution-phase gold nanostar stability, Anal. Bioanal. Chem 410: 6113-6123.

9. Jain PK, Huang X, El-Sayed IX, El-Sayed MA (2008) Noble metals on the nanoscale: Optical and photothermal properties and some applications in imaging, sensing, biology, and medicine. Acc Chem Res 41(12): 1578-1586.

10. Dharmalingam G, Carpenter MA (2017) Chemical sensing dependence on metal oxide thickness for high temperature plasmonics-based sensors. Sensors Actuators B Chem 251: 1104-1111.

11. Karker N, Dharmalingam G, Carpenter MA (2015) Thermal Stability and Energy Harvesting Characteristics of Au Nanorods. Harsh Environment Chemical Sensing 9491: 1-8.

12. Dharmalingam G, Joy NA, Grisafe B, Carpenter MA (2012) Plasmonics-based detection of H_2 and CO: Discrimination between reducing gases facilitated by material control. Beilstein J Nanotechnol 3: 712-721.

13. Karker N, Dharmalingam G, Carpenter MA (2014) Thermal Energy Harvesting Plasmonic Based Chemical Sensors 8(10): 10953-10962.

14. Dharmalingam G, Carpenter MA (2017) Chemical sensing dependence on metal oxide thickness for high temperature plasmonics-based sensors. Sensors Actuators B Chem 251: 1104-1111.

15. Gaspera ED, Guglielmi MG, Perotto S, Agnoli G, Granozzi ML, et al. (2012) CO optical sensing properties of nanocrystalline ZnO-Au films: Effect of doping with transition metal ions. Sensors Actuators B Chem 161: 675-683.

16. Keerthana L, Indhu AR, Dharmalingam G (2022) High-temperature stable plasmonic gold gallia nanocomposites for gas sensing. J Mater Res 38: 497-506.

17. Kondorskiy AD, Lebedev VS (2021) Size and Shape Effects in Optical Spectra of Silver and Gold Nanoparticles. J Russ Laser Res 42: 697-712.

18. Keerthana L, Indhu AR, Dharmalingam G (2022) An approach towards the synthesis of faceted Ga2O3 nano- and micro-structures through the microwave process. Appl Nanosci 12: 2857-2871.

19. Kim B, Park BK (2012) Synthesis of self-aligned tellurium nanotubes by a sodium thiosulfate-assisted polyol method. Electron Mater Lett 8: 33-36.

20. Joy NA, Rogers PH, Nandasiri MI, Thevuthasan S, Carpenter MA (2012) Plasmonic-based sensing using an array of Au-metal oxide thin films. Anal Chem 84: 10437-10444.